Influence of annealing and Al_2O_3 properties on the hydrogen-induced passivation of the Si/SiO_2 interface

G. Dingemans, F. Einsele, W. Beyer, M. C. M. van de Sanden, and W. M. M. Kessels

Citation: Journal of Applied Physics **111**, 093713 (2012);
View online: https://doi.org/10.1063/1.4709729
View Table of Contents: http://aip.scitation.org/toc/jap/111/9
Published by the American Institute of Physics

Influence of annealing and Al_2O_3 properties on the hydrogen-induced passivation of the Si/SiO_2 interface

G. Dingemans,[1] F. Einsele,[2,a)] W. Beyer,[2] M. C. M. van de Sanden,[1] and W. M. M. Kessels[1,b)]
[1]*Department of Applied Physics, Eindhoven University of Technology, P.O. Box 513, 5600 MB Eindhoven, The Netherlands*
[2]*IEK-5, Forschungszentrum Juelich GmbH, 52425 Juelich, Germany*

(Received 5 January 2012; accepted 29 March 2012; published online 7 May 2012)

Annealing at moderate temperatures is required to activate the silicon surface passivation by Al_2O_3 thin films while also the thermal stability at higher temperatures is important when Al_2O_3 is implemented in solar cells with screenprinted metallization. In this paper, the relationship between the microstructure of the Al_2O_3 film, hydrogen diffusion, and defect passivation is explored in detail for a wide range of annealing temperatures. The chemical passivation was studied using stacks of thermally-grown SiO_2 and Al_2O_3 synthesized by atomic layer deposition. Thermal effusion measurements of hydrogen and implanted He and Ne atoms were used to elucidate the role of hydrogen during annealing. We show that the passivation properties were strongly dependent on the annealing temperature and time and were significantly influenced by the Al_2O_3 microstructure. The latter was tailored by variation of the deposition temperature ($T_{dep} = 50\,^{\circ}C$–$400\,^{\circ}C$) with hydrogen concentration [H] between 1 and 13 at.% and mass density ρ_{mass} between 2.7 and 3.2 g/cm^3. In contrast to films with intermediate material properties, the passivation by low- and high density films showed a reduced thermal stability at relatively high annealing temperatures ($\sim 600\,^{\circ}C$). These observations proved to be in good agreement with thermal effusion results of hydrogen and inert gas atoms that were also strongly dependent on film microstructure. We demonstrate that the temperature of maximum effusion decreased for films with progressively lower density (i.e., with increasing [H]). Therefore, the reduced thermal stability of the passivation for low-density hydrogen-rich ([H] $> \sim 5$ at. %) films can be attributed to a loss of hydrogen at relatively low annealing temperatures. In contrast, the lower initial [H] for dense Al_2O_3 films can likely explain the lower thermal stability associated with these films. The effusion measurements also allowed us to discuss the role of molecular- and atomic hydrogen during annealing. © *2012 American Institute of Physics*. [http://dx.doi.org/10.1063/1.4709729]

I. INTRODUCTION

Recombination of charge carriers at silicon surfaces can be a major contributor to suboptimal energy conversion efficiencies of silicon solar cells. In recent years, aluminum oxide (Al_2O_3) thin films, mainly synthesized by atomic layer deposition (ALD) and plasma-enhanced chemical vapour deposition (PECVD), have been used to significantly improve solar cell efficiencies by providing effective surface passivation.[1–11] On both *n*- and *p*-type Si surfaces, Al_2O_3 induces surface recombination velocities, S_{eff}, typically well below 5 cm/s. The effective passivation is related to a significant reduction in defect density at the Si interface ($D_{it} \leq 10^{11}\,eV^{-1}\,cm^{-2}$), after annealing the Al_2O_3 films at relatively low temperatures ($\sim 400\,^{\circ}C$).[12] Simultaneously, the fixed negative charge density associated with the Al_2O_3 films increases up to $Q_f = \sim(3–10) \times 10^{12}\,cm^{-2}$ leading to field-effect passivation through a reduction of the electron density at the Si surface.[5,12]

Recently, Al_2O_3 films have also been applied as capping layers on SiO_2.[13–16] It was found that the advantageous effect of the capping layer was chiefly related to the chemical passivation at the remote interface. Most notably, for stacks comprising SiO_2 synthesized at low-temperatures by PECVD and ALD, very low S_{eff} values < 3 cm/s and low D_{it} values $< 10^{11}\,cm^{-2}\,eV^{-1}$ were obtained,[13,15] which remained stable up to high annealing temperatures.[13] The low defect densities were explained by an effective hydrogenation of defects present at the buried Si/SiO_2 interface under influence of the Al_2O_3 capping layer. Secondary-ion-mass-spectroscopy (SIMS) demonstrated that a fraction of the hydrogen incorporated in the Al_2O_3 during deposition penetrated into SiO_2 and diffused toward the Si/SiO_2 interface during annealing.[14] At this interface, the Si-dangling bond is the most prominent electrically active defect (P_b-type defect).[17–20] As the dangling bond is chemically active, reactions with hydrogen can lead to the elimination of these defects. On the other hand, the fixed charge density responsible for field-effect passivation was found to be very small for thick (e.g., 50–200 nm) thermally-grown SiO_2 layers capped by Al_2O_3.[14,16,21,22] These stacks can therefore be regarded as a model system for studying the chemical

a)Present address: Robert Bosch GmbH, Stuttgart, Germany.
b)Author to whom correspondence should be addressed. Electronic mail: w.m.m.kessels@tue.nl.

passivation induced by Al_2O_3.[14] Moreover, when Al_2O_3 is deposited on H-terminated Si, an interfacial SiO_x is formed.[1] The corresponding electronic interface properties were found to be comparable to other Si/SiO_2 interfaces.[23]

Given the important role of hydrogen in the passivation properties of Al_2O_3, it is vital to explore a number of open questions related to the improvement in chemical passivation during annealing. For example, what is the effect of a variation in annealing temperature and time? What is the influence of the structural properties of Al_2O_3, i.e., mass density and hydrogen concentration, on the diffusion of hydrogen? In what form, atomic or molecular, is hydrogen transported in the Al_2O_3 films? In this paper, these questions will be addressed by the combination of lifetime spectroscopy measurements on SiO_2/Al_2O_3 stacks and thermal effusion measurements.

Thermal effusion measurements have proven to be powerful for studying the material microstructure and hydrogen diffusion in thin films by the detection of volatile species that are released from a film during annealing ($T = 200$ –1100 °C).[24–26] Only recently, effusion measurements have been applied to study the properties of passivation materials.[6,14,27–29] In the context of passivation, effusion measurements are of primary interest as they help to elucidate the important role of hydrogen. It is important to emphasize that the temperature range during the effusion experiments encompasses the activation of the surface passivation, which generally requires annealing at $T = \sim 350$ –450 °C, and also the higher temperature range (>700 °C) typically used during the metallization processes of solar cells. For example, during the manufacture of industrial solar cells with screenprinted contacts, high temperatures ($T > \sim 800$ °C) are typically required and the thermal stability of the passivation film is crucial.[6,30,31] Effusion experiments have, for instance, been applied to study the relation between hydrogen effusion and film composition for *a*-SiN_x:H surface passivation films.[27] In addition, hydrogen effusion from thermally grown SiO_2 exhibited maxima at distinct annealing temperatures, which corresponded with a deterioration in surface passivation quality.[14] For Al_2O_3, the effusion of molecules such as H_2O, H_2, CO, and CO_2 from the film bulk and/or interfaces has been observed in a wide temperature range.[6] In this paper, both the effusion of intrinsic hydrogen species (i.e., originating from H incorporated during deposition) and inert gas atoms which were implanted in Al_2O_3 will be studied.

In this paper, it will be shown that: (i) The hydrogenation of the Si/SiO_2 interface by Al_2O_3 exhibited an Arrhenius behavior as the associated reaction rate increased with increasing annealing temperature. The results suggested that the passivation mechanism of the stacks was not diffusion-limited at annealing temperatures of ~400 °C. (ii) The effusion of hydrogen was strongly influenced by the Al_2O_3 structural properties and the annealing temperature. In addition, the level of passivation achieved at high annealing temperatures was reduced for low-density hydrogen-rich films synthesized at low T_{dep} ($\leq \sim 100$ °C) and for dense films synthesized at high T_{dep} (>300 °C). The cause for the lower thermal stability can be related to the hydrogen transport toward the interface. For the relatively hydrogen-rich films, rapid effusion takes place toward the ambient already at low annealing T, while for dense Al_2O_3 films, a low initial hydrogen density may reduce the effectiveness of interface hydrogenation. (iii) The measurements suggested that hydrogen can diffuse in molecular as well as atomic form, depending on annealing temperature and Al_2O_3 structural properties.

After the experimental details in Sec. II, the annealing kinetics of the SiO_2/Al_2O_3 stacks will be discussed in Sec. III A. Subsequently, the effect of the Al_2O_3 microstructure on the passivation properties will be reported in Sec. III B. The effusion measurements are presented in Sec. III C. The discussion in Sec. IV aims to combine the experimental results to enable a better understanding of the role of hydrogen in the passivation properties of Al_2O_3.

II. EXPERIMENTAL DETAILS

The Al_2O_3 films were synthesized by thermal and plasma ALD in an Oxford instruments OpAL reactor.[8] $Al(CH_3)_3$ served as Al precursor, and either H_2O (thermal ALD) or a remote O_2 plasma (plasma ALD) was employed during the oxidation step. The substrate temperature during deposition T_{dep} was varied between ~50 °C and 400 °C (plasma ALD), to obtain films with different hydrogen content and O/Al ratio.[32] Note that the actual wafer temperature for the films deposited at 300 and 400 °C may be somewhat lower than the substrate temperature. The Al_2O_3 atomic composition was determined by Rutherford backscattering spectroscopy (RBS) and elastic-recoil detection (ERD). High-quality SiO_2 layers with a thickness of ~190 nm were grown by (wet-) thermal oxidation in an H_2O atmosphere at a temperature of ~900 °C. As substrates, floatzone *n*-type Si(100) wafers were used, with a resistivity of ~2 or ~12 Ω cm. After oxidation, no cleaning step was performed prior to Al_2O_3 deposition. To activate the passivation, rapid thermal annealing with a typical ramp-up time of ~30 °C/s was performed in N_2 atmosphere for the SiO_2/Al_2O_3 stacks or in forming gas (10% H_2 in N_2) for single layer SiO_2 reference samples.

Thermal effusion measurements were performed on HF-last Si samples coated on both sides with ~100 nm Al_2O_3 films. The experiments took place in an evacuated quartz tube under high vacuum conditions (10^{-7} mbar) and a linear heating rate of 20 °C/min was used. A quadrupole mass spectrometer was used for the detection of volatile species released from the Al_2O_3 films. Therefore, different masses are detected sequentially at slightly different times and temperatures with a resolution of approximately 20 °C. He and Ne atoms were incorporated in the films by ion implantation. Prior to the measurement, the setup was calibrated by measuring known gas flows of H_2, He, and Ne. More details on the effusion- and implantation experiments can be found elsewhere.[24,33] The passivation properties of the stacks were evaluated by measuring the effective minority carrier lifetime τ_{eff} by the photoconductance decay method (Sinton WCT 100). For each sample, the lifetime was measured for a spot in the middle of the wafer. The *upper limit* of the

surface recombination velocity was calculated from τ_{eff} and is quoted at an injection level of $5 \times 10^{14}\,\mathrm{cm}^{-3}$ by assuming an infinite bulk lifetime, i.e., by employing the relation $S_{eff} < W/(2\tau_{eff})$, with W the wafer thickness of $\sim$200 μm.

III. RESULTS

A. Effect of annealing time and temperature on passivation properties

The injection-level dependent effective lifetime of a SiO_2/Al_2O_3 stack after annealing at a temperature of 400 °C is shown in Fig. 1. The SiO_2/Al_2O_3 stack resulted in a higher effective lifetime of $\tau_{eff} = 2.8$ ms at $\Delta n = 5 \times 10^{14}\,\mathrm{cm}^{-3}$ ($\sim$2 Ω cm *n*-type Si) than obtained for a SiO_2 reference sample annealed in forming gas with $\tau_{eff} = 1.4$ ms. The effective lifetime induced by the stack corresponds to a value of $S_{eff} < 4$ cm/s. In addition, we verified (on different type of wafers) that the passivation performance of the stack was similar to that obtained after "*alnealing*" (annealing the SiO_2 with a sacrificial Al-layer), which is known to lead to an excellent passivation quality.[18,34,35] It was, furthermore, found that annealing in N_2 led to the same passivation performance for the stacks as annealing in forming gas. The observation that the shape of the effective lifetime curves is the same for forming-gas annealed SiO_2 and SiO_2/Al_2O_3 stacks is in accordance with a similar prevailing mechanism underlying the passivation properties, i.e., a high level of chemical passivation.[13,16] The negative Q_f associated with the Al_2O_3 films was found to decrease strongly with SiO_2 interlayer thickness.[15,16] For the thick SiO_2 interlayers of 200 nm used here, the field-effect passivation was found to be insignificant.[14,21] Similar results have recently been reported for SiO_2/*a*-SiN_x:H stacks.[36] It was verified that plasma and thermal ALD Al_2O_3 capping layers resulted in a comparable high level of passivation after annealing (see also Fig. 2). However, prior to annealing, the plasma ALD process led to a significant degradation of the interface quality of the as-grown thermal SiO_2, resulting in effective lifetimes in the microsecond range. This degradation has been attributed to the vacuum UV (VUV) radiation present in the O_2 plasma, which does not play a role during thermal ALD.[12,37,38]

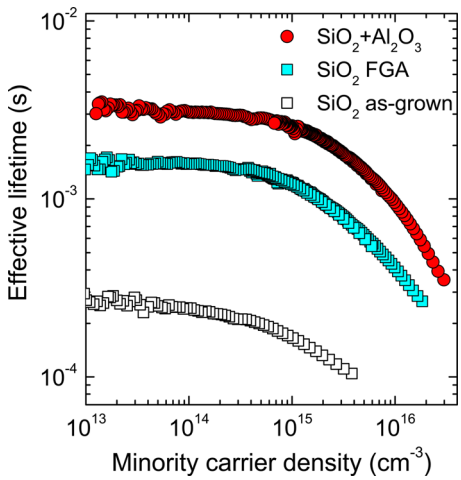

FIG. 1. Injection-level-dependent effective lifetime for a SiO_2/Al_2O_3 stack after annealing at 400 °C (10 min, N_2). As references, data for as-grown SiO_2 and after subsequent forming gas annealing (400 °C, N_2/H_2, 10 min) are shown. The film thickness was $\sim$190 and $\sim$30 nm for SiO_2 and Al_2O_3, respectively. Al_2O_3 was deposited at $T_{dep} = \sim$ 200 °C by thermal ALD. As substrates, $\sim$2 Ω cm *n*-type *c*-Si wafers were used.

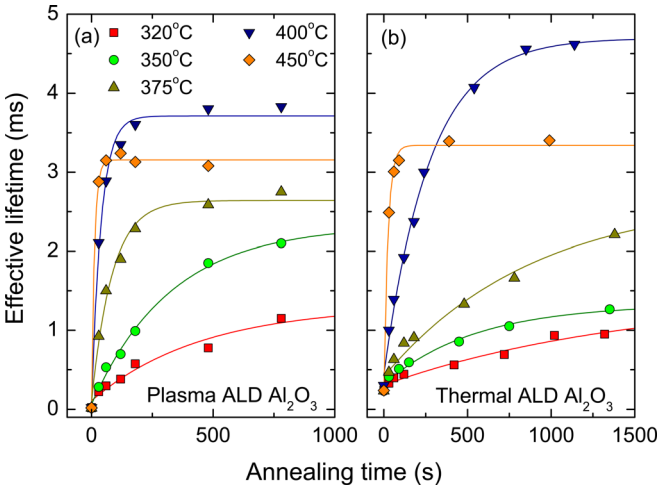

FIG. 2. Effective lifetime ($\Delta n = 5 \times 10^{14}\,\mathrm{cm}^{-3}$) as a function of annealing time for SiO_2/Al_2O_3 stacks. The Al_2O_3 capping films were synthesized by (a) plasma ALD and (b) thermal ALD, using $T_{dep} = 200$ °C. The film thickness was $\sim$190 and $\sim$30 nm for SiO_2 and Al_2O_3, respectively. As substrates, 12 Ω cm *n*-type *c*-Si wafers were used. Annealing took place in N_2. Note the different scale of the horizontal axis in (a) and (b). The lines are exponential fits to the data (see Eq. (1)). For every annealing temperature, a separate sample was used, which was annealed and measured in consecutive steps.

1. Annealing kinetics

To investigate the kinetics associated with the passivation of the SiO_2/Al_2O_3 stacks during annealing, the annealing time and temperature T were varied. Al_2O_3 capping layers synthesized by plasma and thermal ALD are compared in Figure 2. An important observation was that the improvement in the effective lifetime occurred faster for progressively higher annealing temperatures (i.e., Arrhenius behavior). In addition, the level at which the passivation reached a maximum was controlled by the annealing temperature. The highest level of passivation was found for $T = \sim$400 °C, independent of the ALD method applied. However, the annealing time required to reach saturation was longer for Al_2O_3 capping layers synthesized by thermal ALD than by plasma ALD. This difference may be related to a slight difference in structural properties resulting from the two ALD methods.[32] In addition, it is likely that the incorporation of hydrogen into SiO_2 during plasma ALD, as was corroborated by secondary ion mass spectrometry measurements,[14] can also play a role in the observed differences. The comparatively short annealing times associated with plasma ALD capping layers may therefore be partially attributed to the larger hydrogen reservoir in the SiO_2 layer.

Although the passivation performance after annealing at 450 °C was slightly below that obtained at 400 °C, a significant deterioration of the passivation properties occurred only at higher temperatures of 600–700 °C,[14] as will also be discussed later. The degradation depended strongly on the duration of the annealing step. The decrease in surface

passivation quality at elevated T is indicative of an increase in the interface defect density.[14,20,39]

2. Activation energy

To obtain an estimate of the activation energy associated with the passivation kinetics of the stacks, the trends in Fig. 2 were fitted following the approach in Ref. 40 by the expression:

$$\tau_{eff} = [b + a\exp(-t_{anneal}/\tau_{pass})]^{-1}, \quad (1)$$

with t_{anneal} the annealing time. Subsequently, the characteristic time constant τ_{pass} was plotted against $1/k_BT$ to obtain an estimate of the activation energy E_A using the equation

$$\tau_{pass}^{-1} = c\exp(-E_A/k_BT) \quad (2)$$

From the Arrhenius plot in Fig. 3, a value of $E_A = 0.9 \pm 0.2$ eV was determined for plasma ALD capping layers. For thermal ALD, the fitting was less accurate and resulted in $E_A = 1.2 \pm 0.5$ eV. E_A can be regarded as the effective activation energy representative for the processes that lead to the hydrogenation of the interface during annealing.

In the literature, a wide variety of activation energies are reported for the diffusion of hydrogen in SiO_2, but the general understanding is that atomic H and H_2 can rapidly migrate through SiO_2 during annealing.[19,41] For instance, values of $E_A = 0.2$–0.3 eV have been reported by Tuttle *et al.* and Burte *et al.* for atomic H diffusion,[43,44] while Reed *et al.* obtained a higher value of 0.75 eV.[18] For the diffusion of H_2, a value of ~0.5 eV was reported by Fink *et al.*[41] It is generally assumed that the hydrogenation of electronically active defects at the Si/SiO_2 interface is a reaction-limited process rather than diffusion-limited.[18,20,42] The activation energies that we have obtained are higher than the reported activation energies for hydrogen diffusion and, therefore, also suggest that the passivation kinetics of the stacks were not diffusion-limited. Furthermore, the values of E_A fall in the range of earlier reported activation energies during *alnealing* (~1.2 eV) (Ref. 18) and forming gas annealing (~1.5 eV).[20]

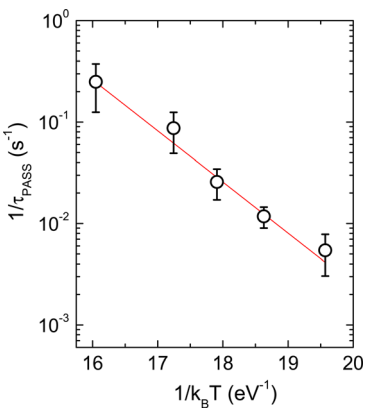

FIG. 3. Arrhenius plot corresponding to Fig. 2(a). τ_{pass} is the time constant corresponding to the increase in the effective lifetime during annealing at temperatures T. An activation energy of $E_A = 0.9 \pm 0.2$ eV was deduced for the passivation kinetics during annealing ($T = 320$-450 °C).

B. Effect of Al_2O_3 structural properties on the passivation

To study the influence of the Al_2O_3 structural properties on the hydrogenation of the Si/SiO_2 interface, Al_2O_3 films were synthesized by plasma ALD at various substrate temperatures ($T_{dep} = 50$–400 °C).[32] Figure 4 shows that the hydrogen content in Al_2O_3 decreased with increasing T_{dep} from approximately 13 at. % (50 °C) to <~1 at. % (~400 °C). Infrared absorption measurements indicated that hydrogen is mostly incorporated as OH groups.[45] For films deposited at $T_{dep} \geq 200$ °C, the O/Al ratio approached the value of ~1.5 representative for stoichiometric Al_2O_3.[32] For lower T_{dep}, the O/Al ratio was observed to increase, which can be partially ascribed to the incorporation of more OH groups. The mass density exhibited an opposite trend to [H] and increased for films deposited at higher T_{dep}. Although less pronounced, an increase was also observed for the total number density of atoms. The observed correlation between the mass density and the hydrogen content shows that both variables cannot be controlled independently by varying the substrate temperature.

The effect of T_{dep} on the passivation quality and the thermal stability of the SiO_2/Al_2O_3 stacks is shown in Figure 5. The level of passivation in the as-deposited state improved with increasing T_{dep}. This effect, albeit less pronounced, has also been reported for as-deposited single-layer Al_2O_3.[32] We attribute the improvement to "*in situ* annealing" (i.e., annealing during deposition) which becomes more effective at higher T_{dep}. During the subsequent post-deposition annealing at 400 °C, the passivation performance of all the stacks improved to values of $S_{eff} < 10$ cm/s, but the impact of annealing was especially significant for $T_{dep} < 300$ °C. The optimal passivation was reached for T_{dep} in the range of 100–200 °C, leading to S_{eff} values < 3 cm/s. However, the optimum in T_{dep} shifted to intermediate values of 200–300 °C, when the annealing temperature was increased up to 600 °C. The passivation performance of the stacks comprising Al_2O_3 deposited at low T_{dep} of 50 °C and 100 °C degraded significantly after annealing at 600 °C. These films exhibited a high hydrogen concentration >~8 at. % and

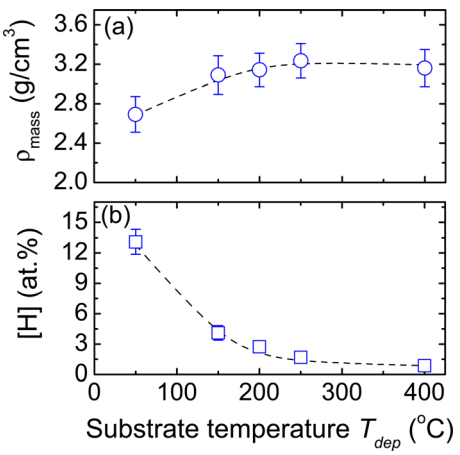

FIG. 4. Mass density ρ_{mass} and hydrogen concentration [H] as a function of T_{dep} for plasma ALD Al_2O_3 films. Data were extracted from RBS and ERD experiments and thickness information from spectroscopic ellipsometry

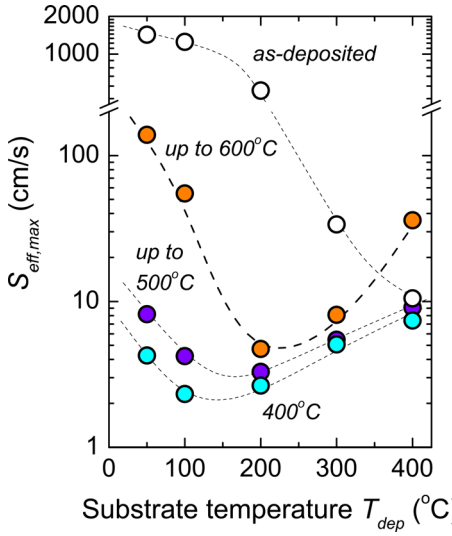

FIG. 5. Thermal stability of SiO_2/Al_2O_3 stacks in terms of the surface recombination velocity $S_{eff,max}$. Al_2O_3 (~30 nm) was synthesized by plasma ALD at various T_{dep}. The five samples were annealed at 400 °C (7 min, N_2), and subsequently annealed in steps of 1 min at 450 °C (not shown), 500 °C and 600 °C. As substrates, 12 Ω cm *n*-type *c*-Si wafers were used. The SiO_2 thickness was 190 nm.

associated low mass density. Moreover, a reduced thermal stability was also observed for the relatively dense film deposited at 400 °C. In conclusion, the observations show that the thermal stability is impaired for Al_2O_3 material properties outside the range of [H] = ~2–6 at. % and $\rho_{mass} = 2.9–3.2$ g/cm^3. A correlation between film density and thermal stability was recently also observed for PECVD SiO_x/SiN_x stacks.[36] It is notable that the range of material properties leading to optimal passivation for Al_2O_3 deposited directly on Si was approximately the same as for the stacks.[32] This underlines the important role of the chemical passivation in the passivation properties of the single-layer Al_2O_3 on Si, as was already reported in our previous work.[32] In Sec. IV, we will show that the passivation results can be related to the significant differences in H effusion observed for Al_2O_3 films of varying composition.

C. Effect of Al_2O_3 microstructure on gas effusion

An important property of the Al_2O_3 film is its microstructure which is likely determining the hydrogen diffusion processes during annealing. The effusion of hydrogen and implanted inert gas atoms was studied to gain insight into the relation between the Al_2O_3 microstructure and hydrogen diffusion.

1. Effusion of H_2, H_2O, and CO_2

Figure 6 shows the effusion signals corresponding to mass-over-charge ratios of $m/z = 2$ (H_2^+) and $m/z = 18$ (H_2O^+) for plasma ALD Al_2O_3 films deposited at various substrate temperatures on Si. Two clear transitions are visible for progressively higher T_{dep}: It is observed that the effusion maxima shifted toward higher annealing temperatures and that the (integrated) signal intensity decreased for progressively higher T_{dep}. A low-temperature peak (LT) and a high temperature peak (HT) (shifted by approximately

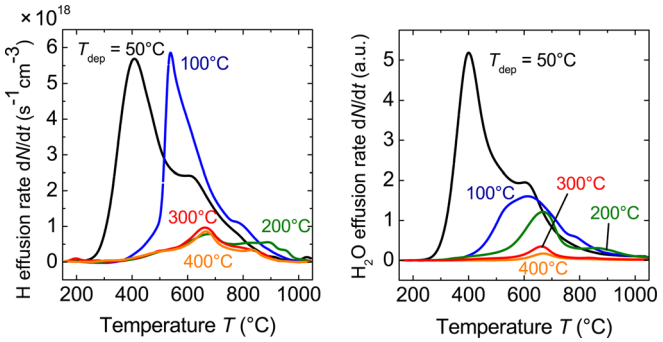

FIG. 6. Effusion measurements of H_2 and H_2O for Al_2O_3 films (thickness ~100 nm) on Si deposited by plasma ALD at various substrate temperatures T_{dep}. The H_2 signal was calibrated by a known H_2 flow. The heating rate during the experiments was 20 °C/min.

200 °C) can be distinguished in the transients of H_2 and H_2O. The annealing temperature that coincides with the LT maxima (T_{LT}) is plotted as a function of T_{dep} in Fig. 7. The LT maxima are observed to shift toward higher annealing temperatures for increasing T_{dep} in the range of 50–200 °C. For dense Al_2O_3 films ($T_{dep} \geq 200$ °C), the position of the LT peak saturated at $T = 680 \pm 40$ °C for H_2 and H_2O. The HT peak also exhibited a saturation behavior. As an important conclusion, the measurements reveal a correlation between the density of the films and the annealing temperature at which the effusion rate of hydrogen is maximum. Moreover, the dependence of the H_2O effusion on the Al_2O_3 microstructure provides evidence that, in addition to surface desorption of adsorbed H_2O molecules, the H_2O signal originated partially from the bulk of the films.

The integrated H_2 effusion signals exhibited a correlation with the initial hydrogen content of the Al_2O_3 films as determined by ERD (Fig. 4). The calibrated H_2 effusion measurements in combination with the initial [H] from ERD enable a quantitative estimate of the percentage of hydrogen released as H_2O. This approach is valid under the assumption that other routes for the release of hydrogen, e.g., CH_x species, can be neglected. In addition, it is notable that the cracking of H_2O has only a minor (typically, <1%) contribution to the H_2^+ signal. We found that the higher T_{dep}, the

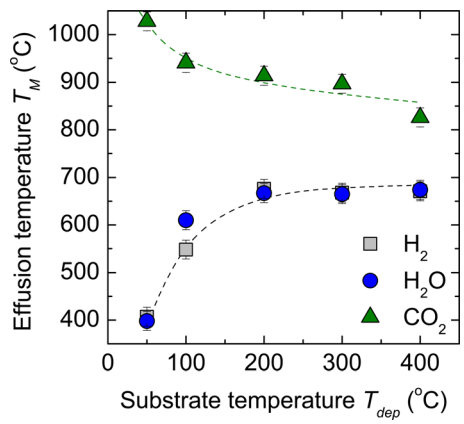

FIG. 7. Temperature of the low-temperature (LT) effusion maxima T_M for plasma ALD Al_2O_3 films synthesized at various T_{dep}. The H_2 and H_2O data correspond to Fig. 6.

smaller the relative contribution of H_2O in the release of hydrogen became (e.g., the fraction released as H_2O was ~60% and ~20% for $T_{dep} = 50\,^{\circ}C$ and 400 °C, respectively). Therefore, the effusion of H_2 appeared to be the prominent route of hydrogen loss for films with low [H] and a relatively high mass density.

As an interesting side note, the effusion maxima of CO_2 ($m/z = 44$) were observed to shift toward lower annealing temperatures for increasing T_{dep}, in contrast to the observations for H_2 effusion (Fig. 7). X-ray diffraction measurements revealed that the Al_2O_3 films crystallize at temperatures between 850 and 900 °C,[46] which is in the range of maximum CO_2 effusion. It is likely that the effusion of carbon impurities coincided with the crystallization of the film. We speculate that a higher annealing temperature is required to crystallize films with lower mass densities, which may explain the trend between CO_2 effusion and T_{dep}. Note that the carbon content of the films was typically <1 at. % ($T_{dep} \geq 200\,^{\circ}C$) as revealed by X-ray photoelectron spectroscopy measurements.

2. Effusion of inert gas atoms

To study the relation between H diffusion and film microstructure in more detail, effusion measurements of implanted He and Ne atoms were carried out. Since implanted inert gas atoms do not form bonds with the host material, the process of out-diffusion is sensitive to variations in the microstructure of the film only, as has previously been demonstrated for materials such as amorphous Si and sputtered ZnO:Al films.[47,48] Here, He and Ne doses of $3 \times 10^{15}\,cm^{-2}$ were implanted in the as-deposited Al_2O_3 films (thickness ~100 nm), with maxima in the distribution at a depth of around 50 nm. For the interpretation of the effusion results, the "onset temperature" T_{onset}, defined as the temperature at which the effusion rate reaches a value of $5 \times 10^{16}\,cm^{-3}\,s^{-1}$, is introduced here in addition to the temperature of maximum effusion rate, T_M. Figure 8 shows the effusion spectra of He and Ne measured for films deposited

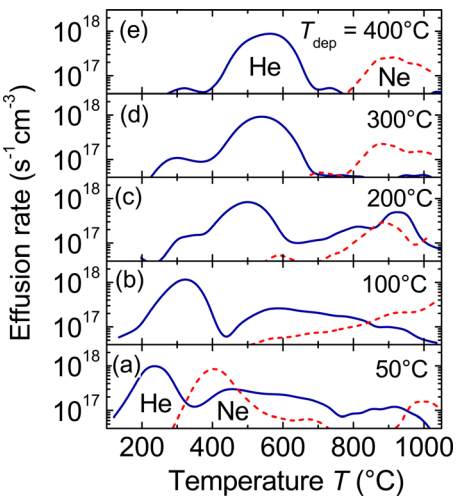

FIG. 8. (a)–(e) The helium (solid lines) and neon (dashed lines) effusion spectra of Al_2O_3 films deposited at different substrate temperatures T_{dep}. The heating rate during the experiments was 20 °C/min.

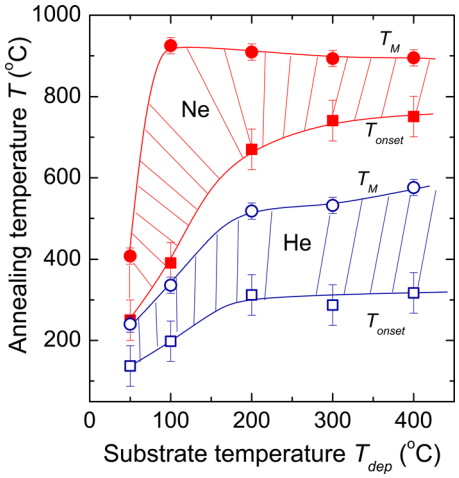

FIG. 9. Ne and He effusion in Al_2O_3 in the plane of the annealing temperature and substrate temperature during deposition T_{dep}. The data correspond to Fig. 8.

at different T_{dep}. The corresponding T_M and T_{onset} are shown in Fig. 9. To activate the effusion, higher annealing temperatures were required for Ne than for He. This is in agreement with the dependence of the diffusion coefficient on the atom size, as will be discussed in Sec. IV. For Al_2O_3 deposited at 50 °C, the effusion spectra exhibited He and Ne peaks at $T_M = 240\,^{\circ}C$ and $T_M = 410\,^{\circ}C$, respectively. For Ne, a sharp increase in T_M (to ~900 °C) was observed for $T_{dep} > 50\,^{\circ}C$, while T_{onset} increased more gradually. For He, the characteristic effusion temperatures also shifted upwards ($T_M = \sim 500\,^{\circ}C$) with increasing T_{dep}. For both He and Ne, the effusion temperatures started to level off at $T_{dep} > \sim 200\,^{\circ}C$. Collectively, the data demonstrate a close correlation between the Al_2O_3 microstructure and the effusion temperature for the inert gas atoms. A similar correlation between T_M and T_{dep} has been reported for a-SiN_x:H films.[27]

IV. DISCUSSION

This section covers the interpretation of the effusion measurements and discusses the correlation between the effusion results and the surface passivation properties during annealing.

A. Simple diffusion model

The effusion of He and Ne can be discussed within the framework of a "doorway diffusion" model. In this classical model, atoms are trapped inside network cages and can only move if the "doorway" opens wide enough by thermal motion.[49] The activation energy of doorway diffusion depends on the radii r and r_D of the atom and "doorway" opening, respectively, and on the shear modulus G of the material

$$E_D = 4\pi^2 G r_D (r - r_D)^2, \quad (3)$$

The corresponding diffusion coefficient D, for a thermally activated out-diffusion process, is given by

$$D(T) = D_0 \exp(-E_D/kT), \quad (4)$$

with D_0 a diffusion prefactor, k the Boltzmann constant, and T the temperature during the effusion experiment. From Eqs. (3) and (4), it follows that the smaller the network openings and/or the "stiffer" the material, the higher is the activation energy E_D and the lower the diffusion coefficient. Moreover, it implies that the diffusion coefficient increases for smaller atoms or molecules. In other words, for a given material, effusion of inert atoms is governed by: (i) the density of the material and (ii) the size of the diffusing species.

B. He and Ne effusion

The observed shift of the effusion maxima of He and Ne toward higher annealing temperatures with increasing T_{dep} (Fig. 9) is indicative of an increase in E_D. When the change in shear modulus G is assumed to be negligible, then Eq. (3) reveals a decrease of the doorway radius r_D for Al_2O_3 synthesized at higher T_{dep}. This decrease in r_D implies a more compact material which is consistent with the evolution of the Al_2O_3 film density as displayed in Fig. 4.

In addition, the observation that the activation energy is higher for Ne than for He diffusion (i.e., $T_M^{Ne} > T_M^{He}$) can be explained by the fact that the size of Ne (atomic radius of ~0.25 nm) is larger than that of He (~0.2 nm).[50] Furthermore, the doorway diffusion model predicts a similar, albeit shifted, trend for He and Ne with T_{dep}. However, T_M^{Ne} (in the range of 900 °C) was virtually independent of T_{dep} in contrast to the trend of He. It is likely that this difference is related to a Ne release process which is governed by significant material reconstruction effects (i.e., crystallisation) and possibly film blistering at elevated temperatures, similar as proposed for CO_2 (see Sec. III C). In this case, the model of doorway diffusion and the correlation between E_D and T_M no longer hold.

C. Hydrogen diffusion

The diffusion of hydrogen is inherently more complex than that of inert gas atoms. For example, hydrogen effusion involves bond breaking and may involve the formation of H_2 through secondary reactions either within the bulk of the material or at the surface/interface. Therefore, the combination of He/Ne and H_2 effusion results may be helpful to explain some of the underlying mechanisms of hydrogen diffusion in Al_2O_3.

The size of a H_2 molecule is assumed to be similar to Ne and larger than the size of He.[51] Therefore, the observation that $T_M^{He} < T_M^{H2}$ is consistent with a higher diffusion coefficient for He, just on the basis of the difference in size. Furthermore, the observation that the effusion of Ne was significant only at high temperatures (above 600 °C for $T_{dep} \geq 200$ °C) suggests that a relatively dense Al_2O_3 structure also impedes the diffusion of similarly-sized H_2 molecules at annealing temperatures below 600 °C. The lower onset temperature of He effusion suggests that atomic H, with a size comparable to He, can diffuse efficiently in a wide range of annealing temperatures (i.e., ~300–550 °C, for $T_{dep} \geq 200$ °C). Note that effusion measurements do not detect atomic H, but always H_2. H_2 arises either from out-diffusion of H_2 molecules or from recombination of atomic H at the film surface, at the film-substrate interface or possibly at internal surfaces (voids). The comparison between the H_2 and He/Ne effusion results leads us to the assumption that diffusion of hydrogen is governed by atomic H as well as by H_2 depending on the Al_2O_3 microstructure and the annealing temperature. Hydrogen diffusion in molecular form is likely more dominant for low-density films and for Al_2O_3 annealed at relatively high temperatures (>600 °C). Diffusion in the form of atomic H might be important for relatively dense Al_2O_3 films, being activated at significantly lower temperatures (between 300 and 600 °C) as a result of its smaller size. A role for atomic H has also been reported for dense a-SiN_x:H films.[27,52,53]

The observation that hydrogen diffusion can take place in Al_2O_3 at relatively low annealing temperatures has been corroborated by secondary ion mass spectrometry depth profiling.[14] Approximately 15% of the hydrogen initially present was released from the Al_2O_3 film during annealing at 400 °C (10 min) either by effusion toward the film surface or by diffusion toward the underlying SiO_2. The observation that hydrogen diffusion can already take place at low annealing temperatures is also consistent with the activation of the passivation performance of the stacks for temperatures as low as ~320 °C (Fig. 2). While atomic as well as molecular hydrogen can diffuse in SiO_2, interface effects, such as pile-up of hydrogen (Ref. 14) and recombination reactions, may play a role in hydrogen diffusion across the SiO_2/Al_2O_3 interface.

The formation of (atomic) hydrogen during annealing can be ascribed to reactions of OH groups with Al atoms, under formation of Al-O bonds. As this bond is very strong, the reaction involved is expected to be very efficient.[54] A similar mechanism was proposed for the release of hydrogen atoms when SiO_2 is capped with an Al layer ("*alnealing*").[18] In fact, it was suggested that a thin AlO_x layer forms at the interface between SiO_2 and Al, under release of hydrogen. On the other hand, generation of H_2 (and H_2O) in the Al_2O_3 bulk may proceed by reactions of two hydroxyls which are in close vicinity, or by (diffusing) atomic hydrogen recombining with a (bonded) hydrogen atom. Note here that the OH groups in Al_2O_3 appear to lead to a more effective hydrogenation than, for example, OH present in deposited or thermally-grown silicon oxides.

Finally, we note that film blistering, i.e., local film delamination, may play a role in the observed effusion signals of H_2/H_2O. The formation of small circular blisters, with a typical diameter of 10–50 micrometers and surface coverage of 5–10%, has also been reported by other authors after (high-temperature) annealing of Al_2O_3 films deposited on Si.[55,56] The exact mechanism responsible for film blistering and the key contributing factors are still under investigation. The cause of blister formation is likely related to local accumulation of H_2 in the film and/or at the interface and an associated pressure built-up and subsequent effusion of gaseous H_2/H_2O.

D. Surface passivation and hydrogenation

Qualitatively, the effusion results are useful in explaining the evolution of the chemical passivation during annealing (Fig. 2). We may expect that the lower level of

passivation obtained for annealing temperatures of ~320 °C can be partially attributed to a low diffusion coefficient of hydrogen. At high temperatures (>600 °C), the depletion of hydrogen from the Al_2O_3 film by H_2/H_2O out-diffusion will lead to a reduction of the hydrogen flux toward the Si interface which can affect the passivation. Enhanced dissociation of interfacial Si-H bonds at relatively high temperatures can exacerbate the effect of the reduced hydrogen content. In fact, passivation and dissociation processes take place in parallel,[20,39] and the equilibrium defect density depends, among others, on the annealing temperature. Therefore, the annealing temperature not only influences the availability of hydrogen but also critically affects the passivation kinetics at the interface directly.

As another important conclusion, the influence of the Al_2O_3 structural properties on hydrogen effusion corresponded well to the passivation results (see Fig. 5). The lower thermal stability for hydrogen-rich Al_2O_3 films ($T_{dep} \leq \sim 100$ °C) can be related to the significant loss of hydrogen from the films already at relatively low annealing temperatures (400–600 °C). For these films, the likelihood of (atomic) hydrogen diffusion toward the Si interface is reduced by a more open film microstructure which also facilitates the formation and release of H_2/H_2O from the Al_2O_3 films. On the other hand, the lower thermal stability for dense Al_2O_3 films ($T_{dep} > \sim 300$ °C) can likely be attributed to the lower initial hydrogen content of the films. The optimal passivation and thermal stability observed for films synthesized at $T_{dep} = \sim 200$ °C can be related to a beneficial combination of high mass density and sufficient hydrogen content. The former controls the diffusion and transport of hydrogen towards the interface, whereas the latter contributes to the availability of hydrogen during thermal processing.

E. Firing stability

The measurements also have implications for Al_2O_3 films implemented in solar cells with screenprinted contacts. The manufacture of these cells involves a firing step at a typical temperature of >800 °C for a few seconds. Firing generally gives rise to an increase in the S_{eff} values relative to the values obtained after annealing Al_2O_3 at moderate temperatures.[6,30,31] The relative decrease in the level of passivation observed at higher annealing temperatures can be attributed mainly to a decrease in the level of chemical passivation.[11] This corresponds to the results in Fig. 5 for the SiO_2/Al_2O_3 stacks exposed to high temperatures. It is interesting to observe in Fig. 6 that the films deposited at $T_{dep} = 200$ °C release hydrogen up to comparatively high annealing temperatures.[6] A clear H_2 effusion feature is observable between 800 and 950 °C, which is absent or significantly smaller for the samples deposited at higher or lower T_{dep}. The hydrogen which is released at high temperatures is expected to favourably influence the level of chemical passivation during firing.

V. CONCLUDING REMARKS

Interface hydrogenation and the associated level of Si surface passivation were found to be strongly dependent on the annealing temperature and on the Al_2O_3 microstructure. Evidence was provided that the passivation kinetics of SiO_2/Al_2O_3 stacks are not limited by the rate of hydrogen diffusion in the Al_2O_3 and SiO_2 layers for relevant annealing temperatures. However, a transition from a low-density and hydrogen-rich Al_2O_3 film to a more dense Al_2O_3 structure was shown to significantly affect the passivation properties and thermal stability. In addition, the Al_2O_3 microstructure critically determined the effusion of hydrogen from the films as a function of the annealing temperature. The variation in hydrogen effusion was consistently associated with the observed variations in the chemical passivation during annealing. For example, the films that showed a high H_2 effusion rate already at comparatively low annealing temperatures exhibited also a significantly lower thermal stability of the corresponding passivation. Furthermore, the results suggested that atomic hydrogen diffusion can take place already at relatively low annealing temperatures and may play a role especially for relatively dense Al_2O_3 films. The conclusion that hydrogen transport mechanisms and the associated interface hydrogenation are critically dependent on film density/microstructure appears to be general to other surface passivation materials. Technologically, our findings can be advantageous for the optimization of passivation schemes comprising Al_2O_3 films in high-efficiency silicon solar cells. The findings in this paper pertaining to the criteria for effective hydrogenation may also have implications for other technologies, for example for bulk passivation of (poly) crystalline materials and hydrogenation of transparent conductive oxides.[57–59]

ACKNOWLEDGMENTS

We thank Dr. P. Engelhart, S. Bordihn (Q-Cells) and N. Terlinden (TU/e) for fruitful discussions. D. Lennartz (IEF-5) and C. van Helvoirt (TU/e) are acknowledged for experimental support. Financial support was received from the German Ministry for the Environment, Nature Conservation and Nuclear Safety (BMU) under Contract No. 0325150 ("ALADIN").

[1]B. Hoex, S. B. S. Heil, E. Langereis, M. C. M. van de Sanden, and W. M. M. Kessels, Appl. Phys. Lett. **89**, 042112 (2006).
[2]G. Agostinelli, A. Delabie, P. Vitanov, Z. Alexieva, H. F. W. Dekkers, S. De Wolf, and G. Beaucarne, Sol. Energy Mater. Sol. Cells **90**, 3438 (2006).
[3]J. Benick, B. Hoex, M. C. M. van de Sanden, W. M. M. Kessels, O. Schultz, and S. W. Glunz, Appl. Phys. Lett. **92**, 253504 (2008).
[4]J. Schmidt, A. Merkle, R. Brendel, B. Hoex, M. C. M. van de Sanden, and W. M. M. Kessels, Prog. Photovoltaics **16**, 461 (2008).
[5]B. Hoex, J. J. H. Gielis, M. C. M. van de Sanden, and W. M. M. Kessels, J. Appl. Phys. **104**, 113703 (2008).
[6]G. Dingemans, R. Seguin, P. Engelhart, F. Einsele, B. Hoex, M. C. M. van de Sanden, and W. M. M. Kessels, J. Appl. Phys. **106**, 114907 (2009).
[7]P. Saint-Cast, D. Kania, M. Hofmann, J. Benick, J. Rentsch, and R. Preu, Appl. Phys. Lett. **95**, 151502 (2009).
[8]G. Dingemans, R. Seguin, P. Engelhart, M. C. M. van de Sanden, and W. M. M. Kessels, Phys. Status Solidi (RRL) **4**, 10 (2010).
[9]S. Miyajima, J. Irikawa, A. Yamada, and M. Konagai, Appl. Phys. Express **3**, 012301 (2010).
[10]B. Vermang, H. Goverde, L. Tous, A. Lorenz, P. Choulat, J. Horzel, J. John, J. Poortmans, and R. Mertens, Prog. Photovolt **20**, 269 (2012).

[11]A. Richter, J. Benick, M. Hermle, and S. W. Glunz, Phys. Status Solidi (RRL) **5**, 202 (2011).
[12]G. Dingemans, N. M. Terlinden, D. Pierreux, H. B. Profijt, M. C. M. van de Sanden, and W. M. M. Kessels, Electrochem. Solid-State Lett. **14**, H1 (2011).
[13]G. Dingemans, M. C. M. van de Sanden, and W. M. M. Kessels, Phys. Status Solidi (RRL) **5**, 22 (2011).
[14]G. Dingemans, W. Beyer, M. C. M. van de Sanden, and W. M. M. Kessels, Appl. Phys. Lett. **97**, 152106 (2010).
[15]G. Dingemans, N. M. Terlinden, M. A. Verheijen, M. C. M. van de Sanden, and W. M. M. Kessels, J. Appl. Phys. **110**, 093715 (2011).
[16]S. Mack, A. Wolf, C. Brosinsky, S. Schmeisser, A. Kimmerle, P. Saint-Cast, M. Hofmann, and D. Biro, IEEE J. Photovoltaics **1**, 135 (2011).
[17]P. J. Caplan, E. H. Poindexter, B. E. Deal, and R. R. Razouk, J. Appl. Phys. **50**, 5847 (1979).
[18]M. L. Reed and J. D. Plummer, J. Appl. Phys. **63**, 5776 (1988).
[19]C. R. Helms and E. H. Poindexter, Rep. Prog. Phys. **57**, 791 (1994).
[20]A. Stesmans, J. Appl. Phys. **88**, 489 (2000).
[21]N. M. Terlinden, G. Dingemans, V. Vandalon, M. C. M. van de Sanden, and W. M. M. Kessels, "Probing the charge density and polarity in dielectric thin films on Si(100) by electric-field-induced second-harmonic generation," (to be published).
[22]J. A. Aboaf, D. R. Kerr, and A. Bassous, J. Electrochem. Soc. **120**, 1103 (1973).
[23]A. Stesmans and V. V. Afanas'ev, Appl. Phys. Lett. **80**, 1957 (2002).
[24]W. Beyer, J. Herion, H. Wagner, and U. Zastrow, Philos. Mag. B **63**, 269 (1991).
[25]W. Beyer and H. Wagner, J. Appl. Phys. **53**(12), 8745–8750 (1982).
[26]W. Beyer, Sol. Energy Mater. Sol. Cells **78**, 235 (2003).
[27]W. Beyer and H. F. W. Dekkers, Mater. Res. Soc. Symp. Proc. **910** (2006).
[28]F. Einsele, W. Beyer, and U. Rau, Phys. Status Solidi C **7**, 1021 (2010).
[29]S. de Wolf, B. Demaurex, A. Descoeudres, and C. Ballif, Phys. Rev. B. **83**, 233301 (2011).
[30]J. Benick, A. Richter, M. Hermle, and S. W. Glunz, Phys. Status Solidi (RRL) **3**, 233 (2009).
[31]J. Schmidt, B. Veith, and R. Brendel, Phys. Status Solidi (RRL) **3**, 287 (2009).
[32]G. Dingemans, M. C. M. van de Sanden, and W. M. M. Kessels, Electrochem. Solid-State Lett. **13**, H76 (2010).
[33]W. Beyer, Phys. Status Solidi C, **1**(5), 1144 (2004).
[34]A. G. Aberle, Prog. Photovoltaics **8**, 473 (2000).
[35]M. J. Kerr and A. Cuevas, Semicond. Sci. Technol. **17**, 35 (2002).
[36]G. Dingemans, M. M. Mandoc, S. Bordihn, M. C. M. van de Sanden, and W. M. M. Kessels, Appl. Phys. Lett. **98**, 222102 (2011).
[37]P. E. Gruenbaum, R. R. King, and R. M. Swanson, J. Appl. Phys. **66**, 6110 (1989).
[38]V. V. Afanas'ev, J. M. M. de Nijs, P. Balk, and A. Stesmans, J. Appl. Phys. **78**, 6481 (1995).
[39]J. H. Stathis, J. Appl. Phys. **77**, 6205 (1995).
[40]J. Mitchel, D. Macdonald, and A. Cuevas, Appl. Phys. Lett. **94**, 162102 (2009).
[41]D. Fink, J. Krauser, D. Nagengast, T. Almeida Murphy, J. Erxmeier, L. Palmetshofer, D. Bräunig, and A. Weidinger, Appl. Phys. A **61**, 381 (1995).
[42]L. Tsetseris and S. T. Pantelides, Phys. Rev. B **70**, 245320 (2004).
[43]B. Tuttle, Phys. Rev. B. **61**, 4417 (2000).
[44]E. P. Burte and P. Matthies, IEEE Trans. Nucl. Sci. **35**, 1113 (1988).
[45]V. Verlaan, L. R. J. G. van den Elzen, G. Dingemans, M. C. M. van de Sanden, and W. M. M. Kessels, Phys. Status Solidi C **7**, 976 (2010).
[46]G. Dingemans, A. Clark, J. A. van Delft, M. C. M. van de Sanden, and W. M. M. Kessels, J. Appl. Phys. **109**, 113107 (2011).
[47]R. Saleh, L. Munisa, and W. Beyer, Sol. Energy Mater. Solar Cells **90**, 3449 (2006).
[48]W. Beyer, J. Hüpkes, and H. Stiebig, Thin Solid Films **516**, 147 (2007).
[49]O. L. Anderson and D. A. Stuart, J. Am. Ceram. Soc. **37**(12), 573 (1954).
[50]*Landolt-Börnstein, Atom- und Molekularphysik I*, edited by A. Eucken (Springer-Verlag, Berlin/Germany, 1950), pp. 325 and 369.
[51]W. Beyer and F. Einsele, *Hydrogen Effusion Experiments, in Advanced Characterization Techniques for Thin Film Solar Cells*, edited by D. Abou-Ras, T. Kirchartz, and U. Rau (Wiley-VCH Verlag GmbH & Co. KGaA, Weinheim, Germany, 2011).
[52]H. F. W. Dekkers, G. Beaucarne, M. Hiller, H. Charifi, and A. Slaoui, Appl. Phys. Lett. **89**, 211914 (2006).
[53]M. Sheoran, D. S. Kim, A. Rohatgi, H. F. W. Dekkers, G. Beaucarne, M. Young, and S. Asher, Appl. Phys. Lett. **92**, 172107 (2008).
[54]S. M. George, Chem. Rev. **110**, 111 (2010).
[55]A. Richter, S. Hennick, J. Benick, M. Hörteis, M. Hermle, and S.W. Glunz, in *Proceedings of the 25th European Photovoltaic Energy Conference*, Valencia, Spain, 2010.
[56]B. Vermang, H. Goverde, A. Lorenz, A. Uruena, G. Vereecke, J. Meersschaut, E. Cornagliotti, A. Rothschild, J. John, J. Poortmans, and R. Mertens, in *Proceedings of the 36th IEEE Photovoltaics Specialists Conference*, Seattle, USA, 2011.
[57]F. Ruske, M. Roczen, K. Lee, M. Wimmer, S. Gall, J. Hüpkes, D. Hrunski, and B. Rech, J. Appl. Phys. **107**, 013708 (2010).
[58]R. Plieninger, H. N. Wanka, J. Kühnle, and J. H. Werner, Appl. Phys. Lett. **71**, 2169 (1997).
[59]F. Duerinckx and J. Szlufcik, Sol. Energy. Mater. Sol. Cells **72**, 231 (2002).